ARTICLES
https://doi.org/10.1038/s41567-021-01429-3
nature physics

Motile dislocations knead odd crystals into whorls

Ephraim S. Bililign[1], Florencio Balboa Usabiaga[2,3], Yehuda A. Ganan[1], Alexis Poncet[4], Vishal Soni[1], Sofia Magkiriadou[1,7], Michael J. Shelley[3,5]✉, Denis Bartolo[4]✉ and William T. M. Irvine[6]✉

The competition between thermal fluctuations and potential forces governs the stability of matter in equilibrium, in particular the proliferation and annihilation of topological defects. However, driving matter out of equilibrium allows for a new class of forces that are neither attractive nor repulsive, but rather transverse. The possibility of activating transverse forces raises the question of how they affect basic principles of material self-organization and control. Here we show that transverse forces organize colloidal spinners into odd elastic crystals crisscrossed by motile dislocations. These motile topological defects organize into a polycrystal made of grains with tunable length scale and rotation rate. The self-kneading dynamics drive super-diffusive mass transport, which can be controlled over orders of magnitude by varying the spinning rate. Simulations of both a minimal model and fully resolved hydrodynamics establish the generic nature of this crystal whorl state. Using a continuum theory, we show that both odd and Hall stresses can destabilize odd elastic crystals, giving rise to a generic state of crystalline active matter. Adding rotations to a material's constituents has far-reaching consequences for continuous control of structures and transport at all scales.

The celebrated interplay between configurational entropy and the energetics of topological defects in two-dimensional melting have provided a lens through which to understand the phases of condensed matter[1–3], such as superfluid films, colloids and liquid crystals[4–9]. Although these systems span a wide range of particle interactions, scales and intermediate phases, they are all unified in that the forces between constituents are primarily longitudinal, their dynamics are equilibrium, and their interactions are symmetric under both time-reversal and parity. What happens if the inter-particle interactions include transverse forces as well[10–18]? This deceivingly minimal generalization can break these assumptions at a fundamental level.

In equilibrium, transverse forces cannot alter the phase behaviour of condensed matter. However, there is no such guarantee out of equilibrium, and such transverse interactions generically occur in collections of naturally and artificially spinning objects. Examples include planetary disks[19], spinning cell aggregates and membrane inclusions[20,21], active colloids and grains[13,17,18,22–27], atmospheric scale dynamics[28,29], parity-breaking fluids[30–35] and simple models of turbulence[36]. Yet to be determined are how this more general and ubiquitous form of matter generically self-organizes, the nature of its stable phases and how it transitions between them.

Figure 1a and Supplementary Video 1 show a ~200×200-μm region within a centimetre-scale monolayer of magnetic colloids. Each particle is uniformly spun by an externally applied magnetic field, resulting in their self-organization into a dynamic and dense phase. The active rotation of the magnets gives rise to both longitudinal magnetic attraction and sustained chiral transverse hydrodynamic interactions, as illustrated in the inset of Fig. 1a. Crucially, the forces are separation-dependent and can be tuned by varying the rotation frequency, providing an ideal platform for exploring how transverse interactions shape the dense phases of chiral matter.

On spinning our particles, we find that the system generically self-organizes into crystal 'whorls'. A snapshot, coloured by the phase of the crystalline bond-orientational order parameter, $\psi_6(\mathbf{x})$ (Fig. 1b and Supplementary Video 2), reveals a polycrystalline arrangement of grains of triangular crystal order separated by topological defects organized into grain boundaries[37]. This picture is reminiscent of metallurgical crystalline phases with quenched disorder; however, unlike their crystalline static counterpart, the structure is continually evolving, and grain boundaries move, collapse and spontaneously emerge as crystalline domains rotate like vortical whorls (Fig. 1c and Supplementary Videos 3 and 12). Segmenting the phase into crystalline domains enables us to study its statistical properties, revealing that, after a short transient, the domains within this polycrystal settle to a constant characteristic size (Supplementary Section 2.2). This scale can be tuned by altering the particle rotation rate alone, yielding either substantially larger or smaller crystalline whorls, as in Fig. 3.

What powers this lively steady state? Careful inspection reveals that the motion of topological defects in the crystalline structure is unlike the familiar motion of dislocations found in conventional passive materials. Conventional dislocations are either stationary or diffuse bidirectionally driven by thermal fluctuations. In our chiral medium, we instead observe that they move ballistically, as shown in Fig. 2a and Supplementary Video 4.

We can gain an intuitive understanding of what powers dislocation motility by inspecting the plastic deformations of the crystal brought about by dislocation glide. As shown in Fig. 2b, dislocation glide reflects the displacement of one crystal plane over the other. As this deformation is equal parts rotation and shear, it is naturally actuated by the rotational drive.

To isolate this phenomenon, we introduce a minimal model of the overdamped dynamics of spinners interacting via transverse,

[1]James Franck Institute and Department of Physics, University of Chicago, Chicago, IL, USA. [2]Basque Center for Applied Mathematics (BCAM), Bilbao, Spain. [3]Center for Computational Biology, Flatiron Institute, New York, NY, USA. [4]Laboratoire de Physique, ENS de Lyon, Université de Lyon, Université Claude Bernard, CNRS, Lyon, France. [5]Courant Institute, New York University, New York, NY, USA. [6]James Franck Institute, Enrico Fermi Institute and Department of Physics, University of Chicago, Chicago, IL, USA. [7]Present address: Laboratory for Experimental Biophysics, Institute of Physics, École Polytechnique Fédérale de Lausanne (EPFL), Lausanne, Switzerland. ✉e-mail: mshelley@flatironinstitute.org; denis.bartolo@ens-lyon.fr; wtmirvine@uchicago.edu

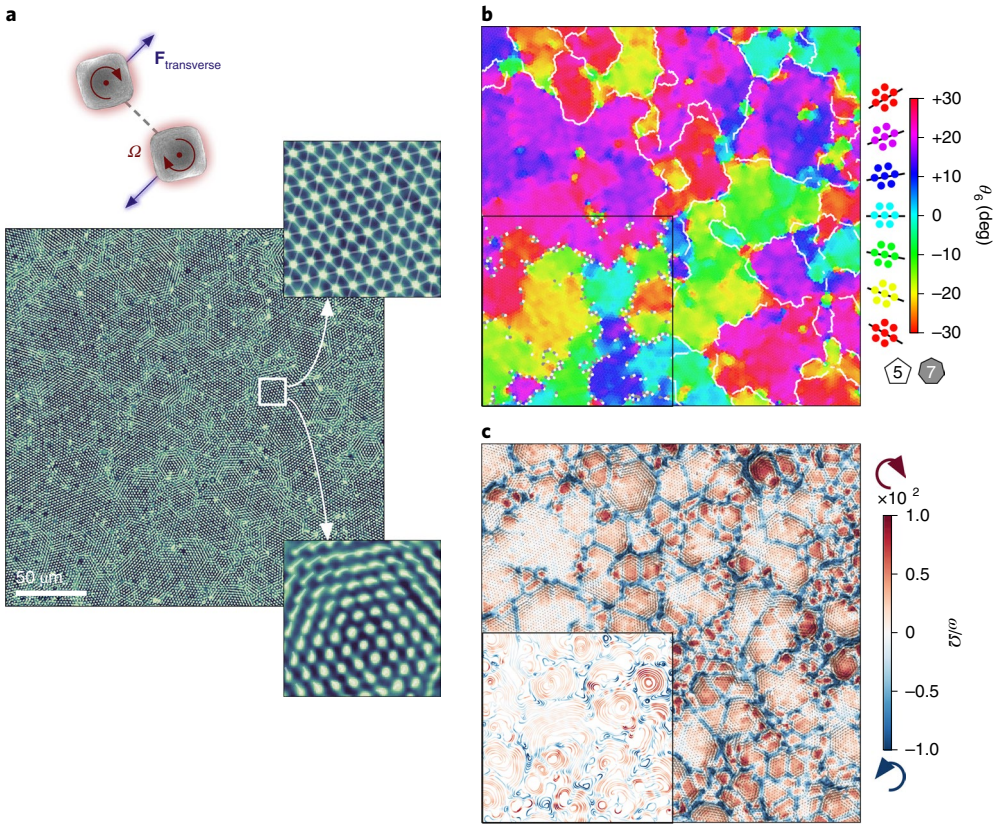

Fig. 1 | A crystal whorl state. a, A dense and dynamic phase of colloids spinning at frequency Ω and interacting through both longitudinal and transverse pairwise interactions is directly imaged with a microscope through crossed polarizers. The rotation-averaged position of each particle appears as a bright spot after background subtraction, time-averaging and blurring, revealing intermittent crystalline order (Supplementary Video 1). Magnifying a region reveals a highly ordered crystalline structure (top), and time-averaging further reveals a rotating flow (bottom). **b**, To further illuminate the polycrystalline structure of this phase, we colour particles by the angle of the local bond-orientational order parameter θ_6=arg(ψ_6). The polycrystal can be segmented into domains, and boundaries are drawn between them (Supplementary Video 2). The inset highlights the individual defects between grains, coloured by the number of neighbours, underlying grain boundaries. **c**, The polycrystal is dynamical and displays intermittent vortical flows, as revealed when each region is coloured by its vorticity ω (Supplementary Video 3). The inset presents the same vortical information through the streamlines of the particle flow (Supplementary Video 12).

frequency-dependent forces and potential longitudinal forces (Supplementary Section 4.1)[38]. This minimal approach is informed by full hydrodynamic simulations of particles that closely approximate our experimental system (Supplementary Section 5.1). The transverse forces arise primarily from near-field hydrodynamic interactions, while the longitudinal interactions arise primarily from both steric repulsion and magnetic attraction (Supplementary Section 5.5).

By initializing simulations with a single dislocation in an otherwise perfectly ordered triangular crystal (Supplementary Videos 5 and 6), we are able to observe the motion of dislocations isolated from interactions with other defects in both minimal and full hydrodynamic simulations. As shown in Fig. 2c, we observe that the glide speed is frequency-dependent. When the longitudinal interactions between particles are isotropic, corresponding to time-averaged magnetic interactions (Supplementary Sections 4.5 and 5.3), the glide velocity is a monotonically increasing function with a threshold (Fig. 2c and Supplementary Section 4.5.1). This is consistent with the notion of a unidirectional propulsion resisted by a local Peierls barrier[39,40]. In the case of anisotropic dipolar interactions, at low frequencies we observe a correction to defect propulsion brought about by a competition between magnetic and rotational interactions (Fig. 2c).

The motility of individual dislocations provides a substantial twist on the collective dynamics of defects normally driven by elastic interactions[41–46]. For example two defects that would normally attract and annihilate in response to elastic forces can instead unbind when propelled by transverse forces, as shown in Fig. 2d.

The collective dynamics of several defects is similarly affected. Figure 2e shows snapshots from simulations in which we initialized a finite-sized grain in an otherwise perfect crystal and varied the rotation frequency (Supplementary Videos 7 and 8). Altering the frequency affects transverse interactions most strongly and thus enables us to tune the balance between stabilizing elastic interactions and defect motility. As shown in Fig. 2e, the grain size is set by the competition between motility and defect interactions. At low rotation frequencies the grains are stable, and their size becomes larger when the defect's propulsion direction is outwards. Similarly, they shrink and collapse for inwards defect motility. When the system is driven sufficiently strongly, the defect motility overpowers the elastic interactions, resulting in unstable grain boundaries.

In the polycrystalline state we observe in our experiments, the instability of grain boundaries results in the exchange of dislocations between adjacent grains, as well as defect proliferation. These nonlinear dynamics drive the system to the dynamical crystal whorl state, erasing any memory of the initial configuration.

The flow field $\mathbf{v}(\mathbf{x}_i)$ that emerges from the combination of motility and proliferation can be readily measured from individual particle trajectories and its corresponding vorticity $\omega(\mathbf{x}_i)$ is shown in Fig. 1c. When time-averaged, this flow field corresponds to a quiet

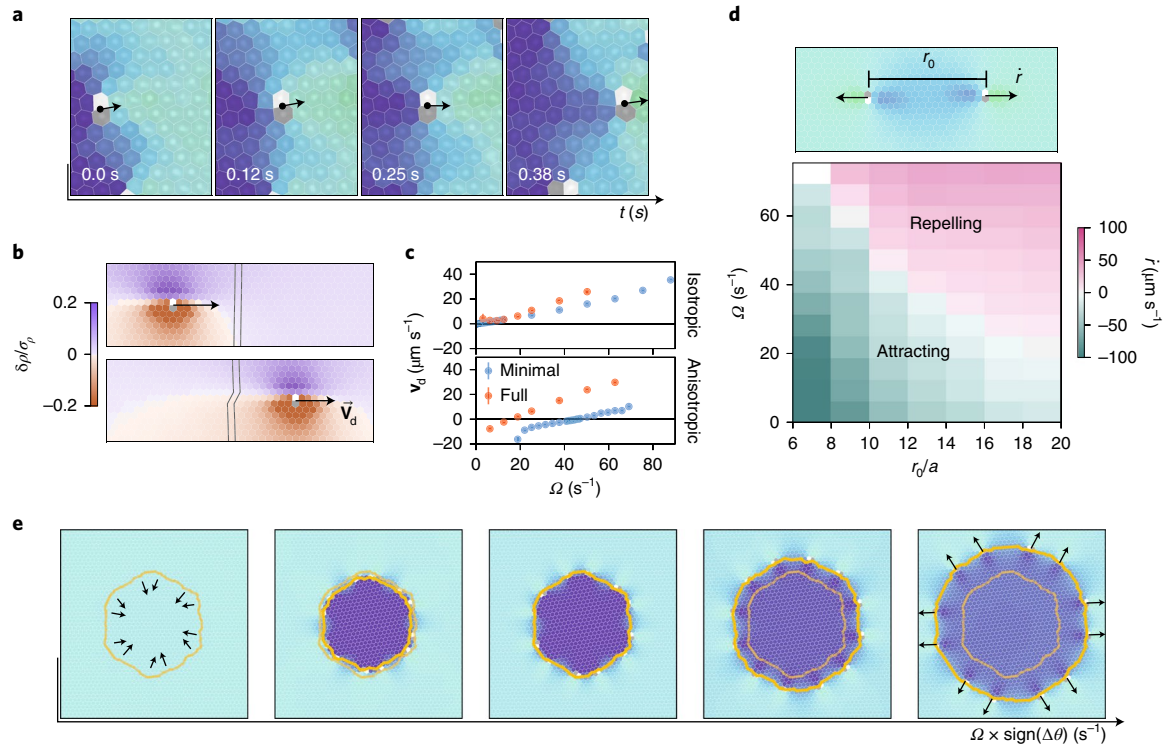

Fig. 2 | Motile dislocations. Dislocations in the chiral crystalline phase behave like active particles. **a**, In the experiment, dislocations are observed to move ballistically in the direction of their Burgers vector. The colourmap is the same as in Fig. 1b. **b**, This behaviour is reproduced in simulations of both the full hydrodynamic and minimal models by initializing a configuration corresponding to a single dislocation in an otherwise undefected crystal. In a crystal of particles interacting via transverse forces, we can intuit the dislocation's direction of motion from the relative displacement of the crystal, which is coloured by the relative density $\delta\rho = \rho - \bar{\rho}$ normalized by the standard deviation σ_ρ (Supplementary Section 2.5). **c**, The precise dislocation speed v_d depends weakly on the details of the interactions. In both the minimal and full hydrodynamic models, the speed increases with frequency for isotropic dipole interactions (top). By contrast, dislocation motility is reversed at a frequency threshold for anisotropic dipole interactions (bottom). Error bars represent the fit covariance (minimal) and standard error (full). **d**, By tuning the frequency Ω and initial separation r_0, two defects that would otherwise attract and annihilate can be made to repel, overwhelming even elastic forces with transverse ones. The colourmap is the same as in Fig. 1b. **e**, The collective dynamics of many defects arranged to form a grain boundary inherits this sensitivity to transverse forces. Such a grain boundary collapses when elastic forces dominate, and expands without bound when transverse forces dominate. The colourmap is the same as in Fig. 1b, and the orange lines indicate the position of the grain boundary in the initial and present states, for comparison.

bulk (Supplementary Section 2.3) and a lively edge[16]. However, our time-resolved measurements reveal instantaneous dynamics shaped by unsteady vortical flows, as illustrated in Fig. 1c. The dynamical and structural pictures of this chiral whorl state are aligned. As seen in Fig. 1b,c, the grain boundaries support strongly localized flows with a vorticity opposite to the particle rotation. By contrast, the grains correspond to low positive vorticity, intermittently interrupted by isolated dislocations zipping through.

In this chaotic stationary state, the balance between even and odd forces remains the controlling parameter that determines the characteristic size of the chiral whorls, which can be viewed through the vorticity in Fig. 3a and the distribution of crystalline grains in Fig. 3b,c (Supplementary Sections 2.2, 2.3, 4.4 and 5.2). The sustained proliferation and annihilation of motile dislocations is reminiscent of active nematics where motile disclinations power spatiotemporal chaos[47]. Here, dislocations give rise to self-kneading crystal whorls.

This self-kneading of the crystal phase results in enhanced mixing, which can be qualitatively captured by artificially tagging the colloids and watching them spread (Fig. 3d and Supplementary Video 11). As shown in Fig. 3e, an artificially dyed blob spreads anisotropically before disintegrating into separate blobs, hinting at a mechanism reminiscent of Richardson diffusion in turbulence. We investigate this quantitatively by tracking the mean-squared separation between pairs of particles in the chiral phase. Figure 3f shows that pair separation is super-diffusive above a separation that corresponds to the characteristic grain size due to a punctuated mix of conventional diffusion within crystalline whorls and Richardson-like diffusion between them. Note that tuning the frequency of rotation alters both the basic unit of time as well as the domain size (Fig. 3d,e), enabling effective diffusion rates to be tuned over orders of magnitude.

To determine whether the crystal whorl state is generic we repeated the experiments shown in Fig. 1 while varying the applied magnetic field strength, adding a static vertical component of magnetic field and varying the shape of the magnetic particles (Supplementary Section 2.6). We also varied the microscopic interactions in our minimal model simulations (Supplementary Section 4.8). Finally, in full hydrodynamic simulations, we simulated spheres and cubes that interact both magnetically and via isotropic attraction potentials (Supplementary Section 5.2). In all cases we find that, when transverse interactions dominate, the system self-organizes into a crystal whorl state, supporting the notion that this state is generic. To gain further insight into the origins of this new state of matter, we adopt a continuum perspective and investigate destabilization mechanisms within this approach. As illustrated in Fig. 4, the microscopic rotational drive induces transverse interactions between the constituent particles that in turn give rise to active stresses in the crystal phase. To gain an essential insight,

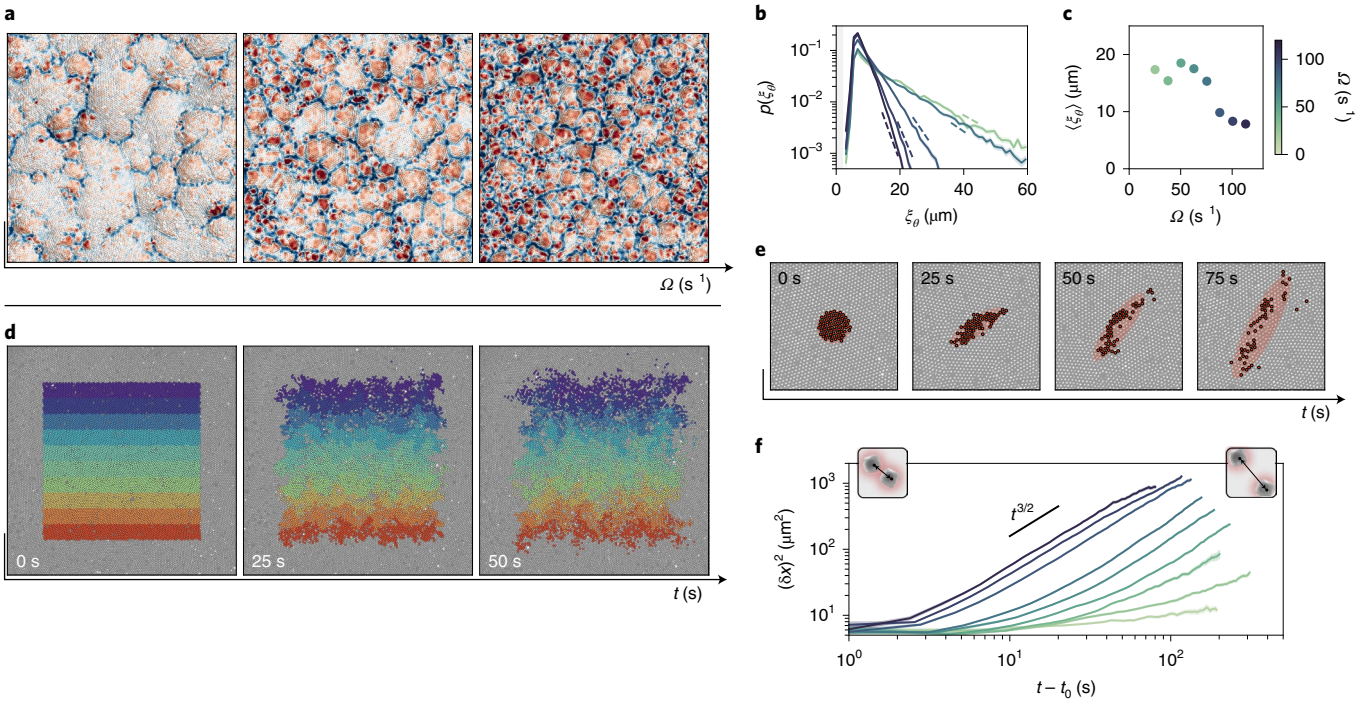

Fig. 3 | Transport in the crystalline whorl state. a, The self-kneading of crystalline patches of material is tunable through the rotation frequency Ω to yield a range of scales. The colourmap is the same as in Fig. 1c. **b**, These states are characterized by an exponential distribution $p(\xi_\theta)$ of grain sizes ξ_θ. Dashed straight lines represent the slope of the associated exponential fit. **c**, Accordingly, the average size of grains in the steady state tends to decrease with frequency. Error bars, which are smaller than markers, represent standard error. **d**, The constant structural kneading of the chiral whorl state by topological defects introduces novel mixing properties that can be imaged by artificially dying stratified layers in a crystal that subsequently bleed into each other. **e**, In contrast to conventional diffusive processes, the smearing of the fluid over time is a strongly anisotropic process, in which an example blob of fluid is pulled apart by the flow between two chiral whorls. **f**, The pairwise separation $(\delta x)^2$ plotted versus time t for particles initially in close proximity suggests that this abnormal spreading gives rise to super-diffusive behaviour, which itself is a function of rotational frequency. Error bars represent standard error.

we first consider the simplified case of a material in which neighbouring particles interact via constant pairwise transverse forces. Figure 4 shows how such interactions naturally give rise to a uniform antisymmetric odd stress[16,48,49], as well as all elastic moduli that can arise in an isotropic solid when energy conservation cannot be assumed[50]. As shown in Fig. 4b,c, the moduli originate geometrically through the changes in perimeter of an infinitesimal material patch. A dilation (Fig. 4b) does not alter the total force on the edge, but increases the perimeter, thereby coupling dilation and rotational stress. Similarly, a shear deformation (Fig. 4c) alternately increases and decreases the length of the edges, giving rise to a rotated shear stress (Supplementary Section 6.2).

The addition of spatial dependence to the interaction forces (Supplementary Section 6.3) makes estimating the moduli more challenging, but it does not alter the basic conclusion that a crystal of spinning particles is a quintessential odd elastic solid. Measuring the deformation field in a collection of nearly circular, monocrystalline droplets (Fig. 4e,f) provides corroborating evidence from experiments and simulations. The droplets rotate at a constant angular velocity that decreases with their radius R. Regardless of the droplet size, they consistently display a radial strain profile that varies from compressive in the centre to dilational on the edge. Within an elastic description, this qualitative feature must originate from odd elastic moduli. A continuum prediction of the strain field (Supplementary Section 7.2) confirms this intuition and predicts the shape of the density profile, as illustrated in Fig. 4d.

A natural question to ask is then whether odd elastic solids powered by odd stresses are linearly stable. We consider the continuum description of an elastic solid with a local displacement $\mathbf{u}(\mathbf{r}, t)$ and local velocity $\mathbf{v}(\mathbf{r}, t)$, that is allowed to experience all stresses consistent with broken parity and time reversal (Supplementary Sections 6.1 and 8.1)[16,50]. In addition to elastic contributions, the symmetric stress includes even and odd viscous contributions $\sigma_{ij} = -p\delta_{ij} + K_{ijkl}\partial_k u_\ell + \eta_{ijkl}\partial_k v_\ell$., where p is the pressure, K_{ijkl} is the elasticity tensor and η_{ijkl} is the viscosity tensor. The inner drive imposed by the spinners is encoded by the antisymmetric stress $\sigma_{ij}^{\mathrm{spin}} = 2\eta_R \epsilon_{ij}\Omega$, where ϵ_{ij} is the Levi-Civita symbol. Ignoring inertia, the dynamics is given by the balance between viscoelastic stresses and substrate drag defined by a constant friction coefficient Γ:

$$\Gamma\mathbf{v} = \nabla\cdot\boldsymbol{\sigma} + \nabla\cdot\boldsymbol{\sigma}^{\mathrm{spin}}, \tag{1}$$

and the continuity equation $\partial_t\rho + \nabla\cdot(\rho\mathbf{v}) = 0$.

Linearizing about a homogeneous quiescent base state $\mathbf{u} = \mathbf{v} = 0$ and $\rho = \rho_0$ and making the ansatz $\mathbf{u}, \mathbf{v}, \rho \propto \exp(-i\omega t + i\mathbf{k}\cdot\mathbf{r})$, we readily obtain an expression for the dispersion $v \equiv \mathrm{Re}(\omega)$ and damping $\alpha \equiv \mathrm{Im}(\omega)$ of displacement and density waves (Supplementary Section 8.2). We find a generic scenario yielding exponential amplification of density fluctuations. A number of different combinations of off-diagonal material parameters in $\boldsymbol{\eta}$ and $\mathbf{K}$ result in different instabilities. However, they all reflect the same mechanistic picture, sketched in Fig. 5a. A density fluctuation is converted to a localized rotation. The resulting net shear across the density fluctuation is in turn converted into an outward force amplifying the initial perturbation, and so on, to defect unbinding. Competition with the stabilizing influence of the conventional bulk and the shear moduli of the elastic solid determine the consistent shape of the dispersion curves shown in Fig. 5a and Supplementary Section 8.2. Crucially, this generic mechanism relies on the coupling between stresses and

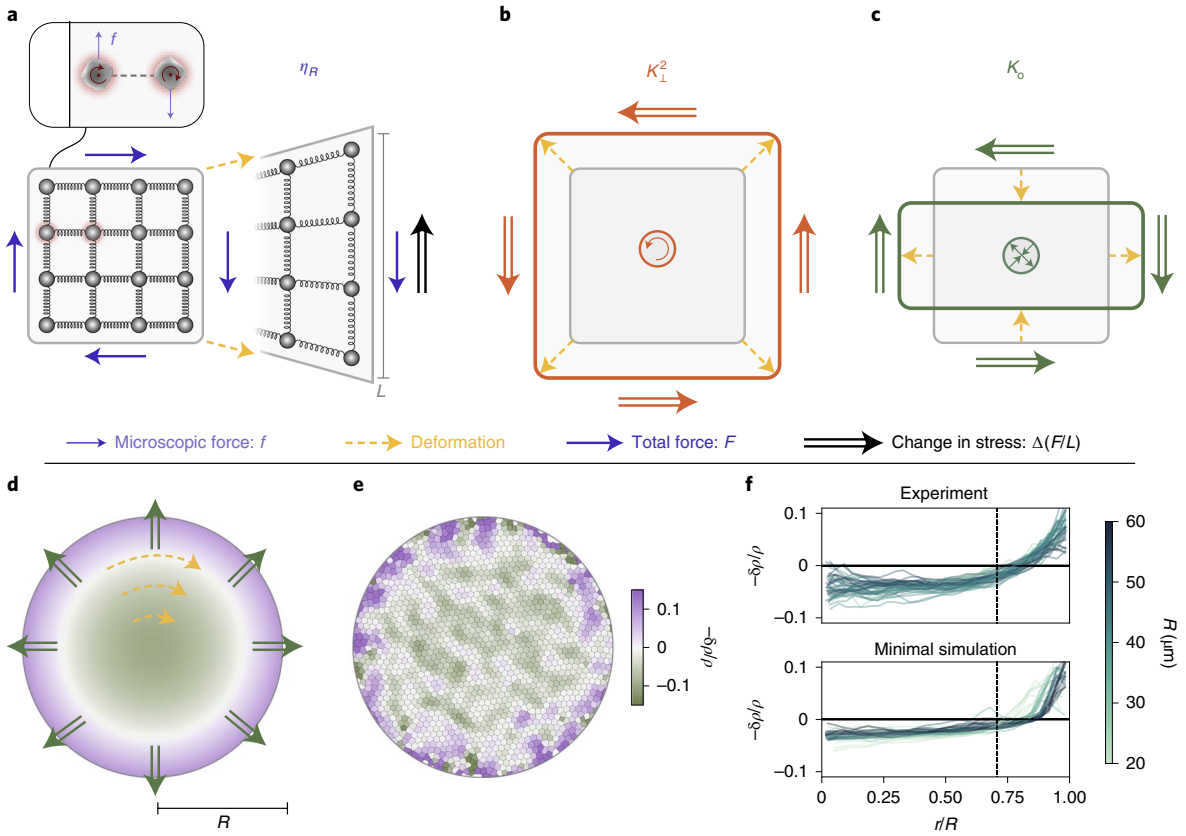

Fig. 4 | Odd response in the steady state. a, A patch of material built of particles that interact with their neighbours via constant, separation-independent transverse forces f parallel to the material's edge sustains a net odd stress $2\eta_R\Omega = nf/L$ on its edge, where n is the number of particles on an edge of length L (see Supplementary Section 6.2 for a more general discussion). On each edge, the macroscopic total force $F = nf$ is unchanged upon dilating the edge, but as the length L of the boundary is increased, there is a net change in stress $\Delta(F/L)$ in a direction opposite to the odd stress. **b**, For a uniform dilation, the deformation leads to a net counter-rotational stress. This coupling between dilation and rotation is denoted by $K_\perp^2$ in the elasticity tensor. **c**, Similarly, for a shear deformation, the system acquires a net rotated shear stress, representative of the odd elasticity K_o. **d**, In a droplet of crystalline material, the odd stress induces a net rotation, balanced by friction with the substrate. The naturally occurring azimuthal distortion generates, via the odd elastic moduli, a characteristic radial density dependence (Supplementary Section 7.2). **e**, We observe this signature of odd elastic response in experiments on droplets by measuring the dilational component of the strain through the relative density $\delta\rho/\rho$. **f**, In both the experiments and simulations, $\delta\rho/\rho$ transitions radially within a droplet from contracting to dilating in a manner independent of droplet radius R. In both cases, we obtain excellent qualitative agreement with the theoretical prediction for the transition radius, denoted by the dashed line (Supplementary Section 7.2).

strains having different spatial symmetries, which is only allowed when time-reversal and parity symmetries are broken at the microscopic level[50,51].

To test this simplified model, we measure the flows $\mathbf{v}(\mathbf{x})$ that occur in the bulk of a large crystallite driven at finite rotation frequency (Supplementary Video 10) and measure the Fourier spectrum of all scalar measures of deformation, including velocity and strain rate (Supplementary Section 2.4). Figure 5b shows that, following the onset of rotations, the azimuthally averaged spectra evolve before eventually settling into a steady state. By comparing the spectra at different times, we extract the mode growth curves shown in Fig. 5 for experiments (Fig. 5c) and simulations (Fig. 5f,g and Supplementary Sections 2.4, 4.8 and 5.4). They reveal the presence of an instability at finite wavelength for all modes with relatively constant growth above a characteristic scale. As shown in Fig. 5c, a spatial map of the integrated growth rate reveals that this instability is consistent with the destabilization of our chiral crystal.

We note, however, that in finite crystalline domains, defects are readily produced at the boundary. Their subsequent propulsion into the bulk could curtail or otherwise affect the full development of the instability. Crucially, we have not observed the spontaneous appearance of defects in the middle of a crystallite in our experiments. These combined observations suggest the existence of an additional mechanism for destabilization in which motile defects nucleate at the boundary and invade the crystal phase, actively fracturing the bulk into whorls.

Our minimal model simulations provide an ideal arena to investigate this possibility. By varying the microscopic interaction parameters, we can tune the system from linearly stable to linearly unstable (Supplementary Section 4.8.1). Remarkably, in both the stable and unstable regimes, we observe that initially perfectly crystalline droplets are destabilized by the production of defects at the edges of the droplets, which subsequently invade the bulk in a visible front (Fig. 5d,e). The only difference is that, deep in the unstable regime (Fig. 5e), we also observe defect nucleation in the bulk of the droplet before the front arrives. Notably, in both cases, a crystal whorl emerges as the steady state (Supplementary Section 4.8.2). This mechanism of destabilization has a different origin from the linear instability described above. Within our continuum approach, the presence of a constant background odd stress plays no role in the crystal's stability—rather, its primary effect is to drive defect propulsion (Supplementary Sections 7.3 and 8.2.1).

Remarkably, measurements of the spectral growth in both regimes, performed for simulations initialized in a polycrystalline

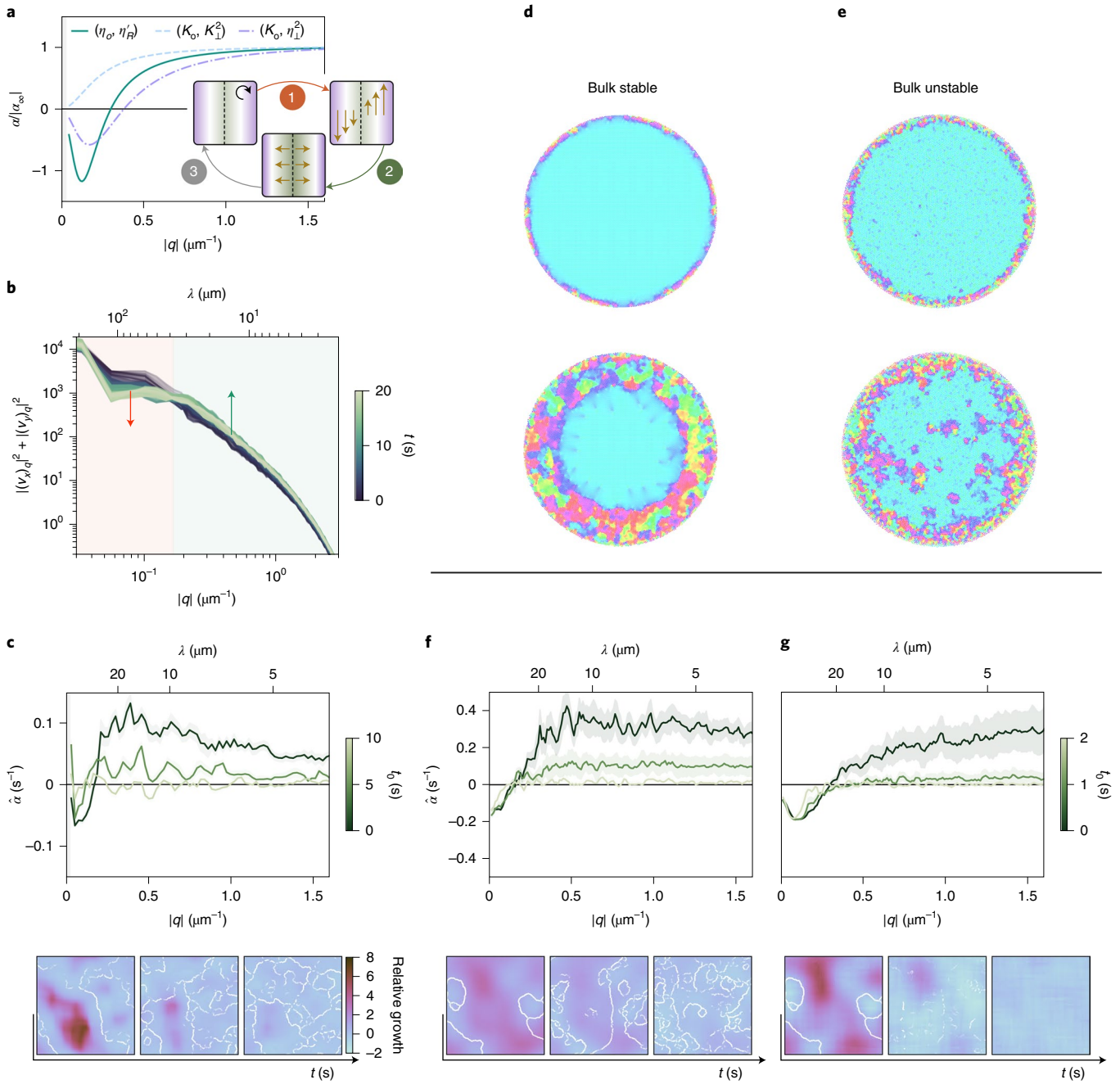

Fig. 5 | Measuring an elasto-hydrodynamic instability. a, The chiral phase responds to a perturbation in spinner density by (1) coupling internal rotations to flow gradients that are (2) transformed into Hall stresses that (3) destabilize the crystal further (Supplementary Section 8.1). A linear stability analysis of this model yields predictions for spectral growth curves arising from the interplay between odd transport coefficients (η_o, K_o) and Magnus-like couplings (η'_R, $K_\perp^2$, $\eta_\perp^2$), whose generic shape we show here. **b**, As the chiral phase approaches the steady state of Fig. 1, we can measure the spectrum of its flow to see decay at large scales and growth at small scales. **c**, The total amount of growth measured at these smaller scales can be mapped over time and compared to the grain boundaries to reveal enhanced growth within initially crystalline patches and vanishing growth at later times (Supplementary Section 2.4). The estimated spectrum of growth $\hat{\alpha}(q)$ reveals stabilization at scales $\lambda \gg \langle \xi_\theta \rangle$ and constant destabilization at scales $\lambda \ll \langle \xi_\theta \rangle$. **d**, In simulations, we tune the inter-particle interaction range to prepare a theoretically stable crystal, for which the crystal is destabilized through dislocation production to reach the whorl state. **e**, Similarly, simulations that are theoretically unstable can become unstable in response to bulk density fluctuations. The colourmap is the same as in Fig. 1b. **f**, The estimated spectrum and spatial map of growth for a theoretically stable simulation resembles the experiment when a polycrystal is destabilized. **g**, The same signatures are observed in a linearly unstable simulation. The colourmaps in **f**,**g** are the same as in **c**.

phase, display general shapes and spatial maps that are similar to those observed in the experiment (Fig. 5f,g). The similar shape of the resulting curves demonstrates the challenge of disentangling the precise origin of the growth in terms of linear response coefficients.

Breaking parity by spinning a material's constituents gives rise to transverse forces that fundamentally alter the organization of matter. Spinner crystals generically melt into a dynamical state driven by motile dislocations. The resulting, tunable crystal whorl state

opens new avenues for the control of structure and transport, from synthetic materials to biological colonies.

Note added in proof: In the concluding stages of our work we became aware of a complementary, independent effort by the groups of N. Fakhri and J. Dunkel who studied parity-breaking crystal dynamics in a bio-physical system (unpublished).

Online content

Any methods, additional references, Nature Research reporting summaries, source data, extended data, supplementary information, acknowledgements, peer review information; details of author contributions and competing interests; and statements of data and code availability are available at https://doi.org/10.1038/s41567-021-01429-3.

Received: 12 March 2021; Accepted: 19 October 2021;
Published online: 16 December 2021

References

1. Jiang, W. et al. Direct observation of the skyrmion Hall effect. *Nat. Phys.* **13**, 162–169 (2017).
2. Jülicher, F., Ajdari, A. & Prost, J. Modeling molecular motors. *Rev. Mod. Phys.* **69**, 1269 (1997).
3. Chaikin, P. M., Lubensky, T. C. & Witten, T. A. *Principles of Condensed Matter Physics* Vol. 10 (Cambridge Univ. Press, 1995).
4. Strandburg, K. J. Two-dimensional melting. *Rev. Mod. Phys.* **60**, 161–207 (1988).
5. Bishop, D. J. & Reppy, J. D. Study of the superfluid transition in two-dimensional ^{4}He films. *Phys. Rev. Lett.* **40**, 1727–1730 (1978).
6. Zahn, K., Lenke, R. & Maret, G. Two-stage melting of paramagnetic colloidal crystals in two dimensions. *Phys. Rev. Lett.* **82**, 2721–2724 (1999).
7. Alsayed, A. M., Islam, M. F., Zhang, J., Collings, P. J. & Yodh, A. G. Premelting at defects within bulk colloidal crystals. *Science* **309**, 1207–1210 (2005).
8. Meng, G., Paulose, J., Nelson, D. R. & Manoharan, V. N. Elastic instability of a crystal growing on a curved surface. *Science* **343**, 634–637 (2014).
9. Thorneywork, A. L., Abbott, J. L., Aarts, D. G. A. L. & Dullens, R. P. A. Two-dimensional melting of colloidal hard spheres. *Phys. Rev. Lett.* **118**, 158001 (2017).
10. Cafiero, R., Luding, S. & Herrmann, H. J. Rotationally driven gas of inelastic rough spheres. *Europhys. Lett.* **60**, 854 (2002).
11. Grzybowski, B. A., Stone, H. A. & Whitesides, G. M. Dynamic self-assembly of magnetized, millimetre-sized objects rotating at a liquid–air interface. *Nature* **405**, 1033–1036 (2000).
12. Yan, J., Bae, S. C. & Granick, S. Rotating crystals of magnetic Janus colloids. *Soft Matter* **11**, 147–153 (2014).
13. Nguyen, N. H., Klotsa, D., Engel, M. & Glotzer, S. C. Emergent collective phenomena in a mixture of hard shapes through active rotation. *Phys. Rev. Lett.* **112**, 075701 (2014).
14. Yeo, K., Lushi, E. & Vlahovska, P. M. Collective dynamics in a binary mixture of hydrodynamically coupled microrotors. *Phys. Rev. Lett.* **114**, 188301 (2015).
15. Kokot, G., Piet, D., Whitesides, G. M., Aranson, I. S. & Snezhko, A. Emergence of reconfigurable wires and spinners via dynamic self-assembly. *Sci. Rep.* **5**, 9528 (2015).
16. Soni, V. et al. The odd free surface flows of a colloidal chiral fluid. *Nat. Phys.* **15**, 1188–1194 (2019).
17. Shen, Z. & Lintuvuori, J. S. Two-phase crystallization in a carpet of inertial spinners. *Phys. Rev. Lett.* **125**, 228002 (2020).
18. Liu, P. et al. Oscillating collective motion of active rotors in confinement. *Proc. Natl Acad. Sci. USA* **117**, 11901–11907 (2020).
19. Armitage, P. J. Turbulence and angular momentum transport in a global accretion disk simulation. *Astrophys. J. Lett.* **501**, L189 (1998).
20. Petroff, A. P., Wu, X.-L. & Libchaber, A. Fast-moving bacteria self-organize into active two-dimensional crystals of rotating cells. *Phys. Rev. Lett.* **114**, 158102 (2015).
21. Oppenheimer, N., Stein, D. B. & Shelley, M. J. Rotating membrane inclusions crystallize through hydrodynamic and steric interactions. *Phys. Rev. Lett.* **123**, 148101 (2019).
22. van Zuiden, B. C., Paulose, J., Irvine, W. T. M., Bartolo, D. & Vitelli, V. Spatiotemporal order and emergent edge currents in active spinner materials. *Proc. Natl Acad. Sci. USA* **113**, 12919–12924 (2016).
23. Aubret, A., Youssef, M., Sacanna, S. & Palacci, J. Targeted assembly and synchronization of self-spinning microgears. *Nat. Phys.* **14**, 1114–1118 (2018).
24. Snezhko, A. Complex collective dynamics of active torque-driven colloids at interfaces. *Curr. Opin. Colloid Interface Sci.* **21**, 65–75 (2016).
25. Scholz, C., Engel, M. & Pöschel, T. Rotating robots move collectively and self-organize. *Nat. Commun.* **9**, 931 (2018).
26. Kokot, G. et al. Active turbulence in a gas of self-assembled spinners. *Proc. Natl Acad. Sci. USA* **114**, 12870–12875 (2017).
27. Lim, M. X., Souslov, A., Vitelli, V. & Jaeger, H. M. Cluster formation by acoustic forces and active fluctuations in levitated granular matter. *Nat. Phys.* **15**, 460–464 (2019).
28. Bouchet, F. & Venaille, A. Statistical mechanics of two-dimensional and geophysical flows. *Phys. Rep.* **515**, 227–295 (2012).
29. Baroud, C. N., Plapp, B. B., She, Z.-S. & Swinney, H. L. Anomalous self-similarity in a turbulent rapidly rotating fluid. *Phys. Rev. Lett.* **88**, 114501 (2002).
30. Korving, J., Hulsman, H., Knaap, H. & Beenakker, J. Transverse momentum transport in viscous flow of diatomic gases in a magnetic field. *Phys. Lett.* **21**, 5–7 (1966).
31. Hoyos, C., Moroz, S. & Son, D. T. Effective theory of chiral two-dimensional superfluids. *Phys. Rev. B* **89**, 174507 (2014).
32. Wiegmann, P. & Abanov, A. G. Anomalous hydrodynamics of two-dimensional vortex fluids. *Phys. Rev. Lett.* **113**, 034501 (2014).
33. Souslov, A., Dasbiswas, K., Fruchart, M., Vaikuntanathan, S. & Vitelli, V. Topological waves in fluids with odd viscosity. *Phys. Rev. Lett.* **122**, 128001 (2019).
34. Banerjee, D., Souslov, A., Abanov, A. G. & Vitelli, V. Odd viscosity in chiral active fluids. *Nat. Commun.* **8**, 1573 (2017).
35. Han, M. et al. Fluctuating hydrodynamics of chiral active fluids. *Nat. Phys.* **17**, 1260–1269 (2021).
36. Eyink, G. L. & Sreenivasan, K. R. Onsager and the theory of hydrodynamic turbulence. *Rev. Mod. Phys.* **78**, 87 (2006).
37. Lavergne, F. A., Aarts, D. G. & Dullens, R. P. Anomalous grain growth in a polycrystalline monolayer of colloidal hard spheres. *Phys. Rev. X* **7**, 041064 (2017).
38. Anderson, J. A., Glaser, J. & Glotzer, S. C. HOOMD-blue: a Python package for high-performance molecular dynamics and hard particle Monte Carlo simulations. *Comput. Mater. Sci.* **173**, 109363 (2020).
39. Peierls, R. Reports on progress of physics. *Phys. Soc.* **VI**, 78 (1939).
40. Nabarro, F. Dislocations in a simple cubic lattice. *Proc. Phys. Soc.* **59**, 256 (1947).
41. Schall, P., Cohen, I., Weitz, D. A. & Spaepen, F. Visualization of dislocation dynamics in colloidal crystals. *Science* **305**, 1944–1948 (2004).
42. Weinberger, C. R. & Cai, W. Surface-controlled dislocation multiplication in metal micropillars. *Proc. Natl Acad. Sci. USA* **105**, 14304–14307 (2008).
43. Irvine, W. T. M., Hollingsworth, A. D., Grier, D. G. & Chaikin, P. M. Dislocation reactions, grain boundaries and irreversibility in two-dimensional lattices using topological tweezers. *Proc. Natl Acad. Sci. USA* **110**, 15544–15548 (2013).
44. Amir, A. & Nelson, D. R. Dislocation-mediated growth of bacterial cell walls. *Proc. Natl Acad. Sci. USA* **109**, 9833–9838 (2012).
45. Deutschländer, S., Dillmann, P., Maret, G. & Keim, P. Kibble-Zurek mechanism in colloidal monolayers. *Proc. Natl Acad. Sci. USA* **112**, 6925–6930 (2015).
46. Braverman, L., Scheibner, C. & Vitelli, V. Topological defects in non-reciprocal active solids with odd elasticity. Preprint at https://arxiv.org/abs/2011.11543 (2020).
47. Sanchez, T., Chen, D. T., DeCamp, S. J., Heymann, M. & Dogic, Z. Spontaneous motion in hierarchically assembled active matter. *Nature* **491**, 431–434 (2012).
48. Dahler, J. S. & Scriven, L. E. Theory of structured continua. I. General consideration of angular momentum and polarization. *Proc. R. Soc. Lond. A Math. Phys. Eng. Sci.* **275**, 504–527 (1963).
49. Tsai, J.-C., Ye, F., Rodriguez, J., Gollub, J. P. & Lubensky, T. C. A chiral granular gas. *Phys. Rev. Lett.* **94**, 214301 (2005).
50. Scheibner, C. et al. Odd elasticity. *Nat. Phys.* **16**, 475–480 (2020).
51. Epstein, J. M. & Mandadapu, K. K. Time-reversal symmetry breaking in two-dimensional nonequilibrium viscous fluids. *Phys. Rev. E* **101**, 052614 (2020).

Data availability

The data contained in the plots within this paper and other findings of this study are available from the corresponding author on reasonable request.

Code availability

The minimal model simulations were performed using freely available HOOMD-Blue codes[38]. Hydrodynamic simulations were carried out using codes based on the publicly available code at https://github.com/stochasticHydroTools/RigidMultiblobsWall. Input files are available on request to the authors.

Acknowledgements

We acknowledge discussions with P. Wiegmann, A. Abanov, D. Nelson, C. Scheibner, M. Han, M. Fruchart, S. Gokhale, N. Fakhri and J. Dunkel. We thank V. Vitelli for an insightful discussion on the importance of odd stress on defect motility. We thank W. Yan for useful conversations. This work was primarily supported by the University of Chicago Materials Research Science and Engineering Center, which is funded by the National Science Foundation (NSF) under award no. DMR-2011854. Additional support was provided by NSF DMR-1905974, NSF EFRI NewLAW 1741685 and the Packard Foundation. M.J.S. acknowledges support from NSF grants DMR-1420073 (NYU-MRSEC) and DMR-2004469. D.B. acknowledges support from ARN grant WTF and IdexLyon Tore. E.S.B. was supported by the National Science Foundation Graduate Research Fellowship under grant no. 1746045. D.B. and W.T.M.I. gratefully acknowledge support from the Chicago-France FACCTS programme. F.B.U. acknowledges support from 'la Caixa' Foundation (ID 100010434), fellowship LCF/BQ/PI20/11760014 and from the European Union's Horizon 2020 research and innovation programme under Marie Skłodowska-Curie grant agreement no. 847648. The University of Chicago's Research Computing Center and the University of Chicago's GPU-based high-performance computing system (NSF DMR-1828629) are acknowledged for access to computational resources and the Chicago MRSEC (US NSF grant no. DMR-2011854) for access to its shared experimental facilities.

Author contributions

E.S.B. designed and performed experiments and analysed data. Y.A.G. designed and performed minimal model simulations and elastic theory. F.B.U. designed and performed fully hydrodynamic simulations. V.S. and S.M. contributed to experiments and analytical tools. A.P., D.B., Y.A.G., E.S.B., W.T.M.I. and M.J.S. performed continuum modelling. W.T.M.I., D.B. and M.J.S. designed and supervised research. All authors discussed the results and analysis.

Competing interests

The authors declare no competing interests.

Additional information

Supplementary information The online version contains supplementary material available at https://doi.org/10.1038/s41567-021-01429-3.

Correspondence and requests for materials should be addressed to Michael J. Shelley, Denis Bartolo or William T. M. Irvine.

Peer review information *Nature Physics* thanks Juho Lintuvuori and the other, anonymous, reviewer(s) for their contribution to the peer review of this work.